

SAE Paper Number 2022-01-1069©2022 Society of Automotive Engineers International. This paper is
Posted on this website with permission from SAE International. As a user of this website you are
Permitted to view this paper on-line and print one copy of this paper for your use only. This paper
may not be copied, distributed or forwarded without permission from SAE.



Investigations Regarding the Causes of Filter Blocking in Diesel Powertrains

Jim Barker Innospec

Graham Langley, Anastarsia Carter, and Julie Herniman University of Southampton

Jacqueline Reid and Ed Wilmot Innospec

Citation: Barker, J., Langley, G., Carter, A., Herniman, J. et al., "Investigations Regarding the Causes of Filter Blocking in Diesel Powertrains," SAE Technical Paper 2022-01-1069, 2022, doi:10.4271/2022-01-1069.

Received: 01 May 2022

Revised: 23 Jun 2022

Accepted: 27 Jun 2022

Abstract

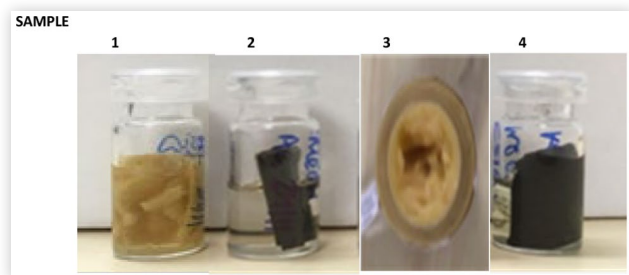
Developed by Rudolph Diesel in the 1890s, the diesel powertrain is used in many applications worldwide. For significant time the engine fuel source for these engines was petroleum diesel, until new legislation regarding emission reduction and smog mitigation saw the introduction of petroleum diesel and biodiesel (Fatty acid methyl ester; FAME) blends in the early 2000s. Since then there have been many instances of filters in diesel powertrains across heavy, light and off-road platforms becoming blocked with unidentified material, for example in the United States, Northern Europe and Scandinavia. Filters are designed to remove contaminants from the fuel system and as the filter becomes plugged it restricts the fuel flow resulting in loss of engine

power and eventual breakdown. Understanding The nature of the material responsible for such blockages is clearly important to the industry and has been the subject of many studies. However, it is also clear from such work that not all the materials responsible for filter blocking have been identified. This work will describe the application of a variety of mass spectrometry techniques such as Fourier Transforms Ion Cyclotron Mass Spectrometry (FT-ICR-MS); Ultrahigh Performance Supercritical Fluid Mass Spectrometry. (UHPSFC-MS) to further identify the filter blocking materials in conjunction with more traditional analytical techniques for example Scanning Electron Microscopy, (SEM), X-ray Fluorescence Spectroscopy (EDS) and Fourier Transform Infra-red Microscopy (FTIRM).

Introduction

As the fuel economy moves towards the low carbon goal, the use of FAME is an integral part of that process. Concurrent with this has been the emissions legislation driven introduction of the high-pressure common rail diesel engine which because of its highly engineered tolerances requires protection from particles in fuel and the introduction of ultra-low sulfur diesel (ULSD). The uninterrupted flow of fuel through filter systems associated with common rail powertrains is fundamental to its ability to control emissions. Anything which compromises this is of concern, as the filter blocking or restriction results in fuel starvation to the engine, loss of power, stalling, misfire, loss of economy, increased emissions or complete breakdown. Since the introduction ULSD, biodiesel and biodiesel blends there have been increased reports of fuel filter flow restriction and blocking in diesel vehicles worldwide [1, 2, 3]. This has led to concomitant studies as many of the filter blocking problems in the field have led back to impurities in FAME these have been attributed to both "soft" particles; such as sterol glucosides and "hard" particles; for example, sodium sulfate. Fersner et al. [4] used the standard method

ASTM D2068 filter blocking tendency [5] to show that sterol glucosides caused filtration problems at the ppm level. Jolly also found the impurities in biodiesel caused filter blocking in field samples [6], and Gopalan [7] showed the importance of degradation products. Barker [8] and Richards [9] identified biodiesel origin acids on filters, and recent work by Heiden [10] has introduced a cooling step to known analytical protocols to help with interferences found when petrodiesel is present. The work regarding filter blocking incidents has led to specifications for biofuels CEN14214:2011 [11] and ASTM D6751-20a [12] being tightened and new methods developed to analyze impurity componentry in biodiesel, for example saturated mono-glycerides by gas chromatography EN17057 [13], but the majority of methods cannot be used for a petrodiesel/biodiesel blends. The complex nature and constant changing landscape of components in fuels has seen an ineluctable increase in the complexity and number of filter blocking incidents. The biodiesel (BD) used may now come from waste products or seed oils, extending the impurity profile of insoluble material. ULSD may see variation in its constituent ratios, for example aromatic to aliphatic which

FIGURE 1 Filter Samples

can severely impact its ability to solubilize and “transport” impurities (13-14). The trend towards the replacement of high carbon content petrodiesel by biodiesel usage continues to grow, driven by the benefits to air pollution reduction, life cycle and reduction in the use of crude oil. Investigations and development of methodologies to determine and characterize impurities in FAME are still required to assist the industry in managing this. The analytical technique of mass spectrometry is well placed to characterize these materials and methodology will be described here that is rapid, can be used in the presence of petrodiesel, and delivers molecular identification without needing an expensive or difficult to source suite of standards.

Methods and Samples

Fuel Filters

These were sourced from vehicle failures in Europe and consisted of examples from light and medium duty vehicles, see [Figure 1](#). The vehicles were fueled with petrodiesel/biodiesel blends, mileage was varied, and engine failure resulted due to blocked filters.

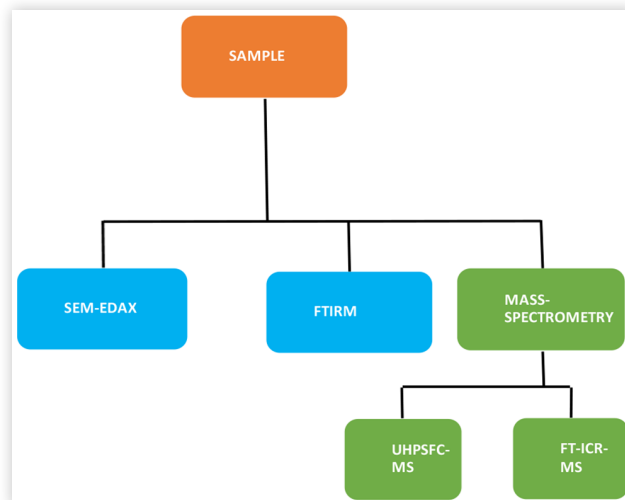
Sample Preparation

A 1 cm square of each fuel filter was put into a vial with ~1 mL of methanol (shown in [Figure 1](#)). One drop of the infused methanol was taken immediately and diluted into 1 mL methanol for direct infusion positive and negative ion (ESI FT-ICR MS) analysis. The addition of formic acid or ammonia solution to each sample was utilized on occasion to force protonation (positive ion ESI) and deprotonation (negative ion ESI) of species respectively, prior to further analysis by direct infusion positive and negative ion ESI FT-ICR MS method. A 1 cm square of each sample was placed into a vial with 1 mL of methanol, the undiluted infused methanol was then analyzed by positive and negative ion ESI UHPSFC-MS.

Note one filter was very soiled and a sample was scraped from the surface and placed in the methanol.

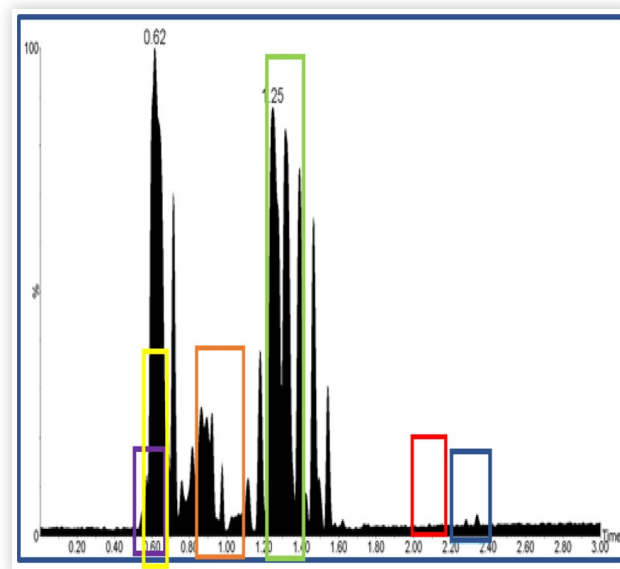
The purpose of this study was to explore the use of mass spectrometry to screen material found on “field” filter samples

of FAME origin using the protocol highlighted in green in [Figure 2](#) below.

FIGURE 2 Simplified Protocol for Analysis of Fouled Filters

The samples were screened for the listed compounds:

- Fatty acid methyl esters (FAMES)
- Fatty acid methyl ester (FAME) oxidation products
- Free fatty acids (FFAs)
- Sterol glucosides (SGs)
- Monoacylglycerols (MAGs)
- Fatty acid sterol esters (FASEs)

FIGURE 3 Typical filter extract Positive ion ESI UHPSFC-MS BPICC with boxes indicating the regions associated with the impurities.

Analysis

One example of each compound found to be present within the fuel filters will be shown in detail, using positive and negative ion (ESI UHPSFC-MS) and FT-ICR MS data.

The mass spectral and other techniques have been described in detail previously in other SAE papers [15,16].

The key findings of each fuel filter sample will be discussed with similarities between fuel filter samples outlined, and the filters grouped by compounds present. A detailed example will be given for each chemical group investigated. A typical example base peak ion current chromatogram (BPICC) is shown in [Figure 3](#) and the relevant areas of interest described. The reconstructed ion current chromatograms (RICCs) of each impurity of interest are described in [Figure 4](#).

Fatty Acid Methyl Esters (FAMES) The fuel filter number F4 Southern Europe, medium duty will be used as the example to illustrate the presence of FAMES within fuel filter samples.

[Table 1](#) shows a summary of FAMES to be screened for, their respective molecular formulae and structures, adducts that can be present and their associated masses. Nominally isobaric species are in bold and underlined.

[Figure 3](#) shows a general example of a positive ion ESI UHPSFC-MS BPICC of a fuel filter, with coloured boxes showing impurity regions of interest further detail in [Table 1](#), the yellow box highlighting chromatographic peaks within the region of retention found for FAMES (t_R 0.55-0.70 min).

The corresponding positive ion ESI UHPSFC-MS mass spectrum shown in [Figure 5](#), shows ammoniated molecules

FIGURE 4 ESI UHPSFC-MS RICCs and BPICCs of impurities with pale blue box highlighting region of interest.

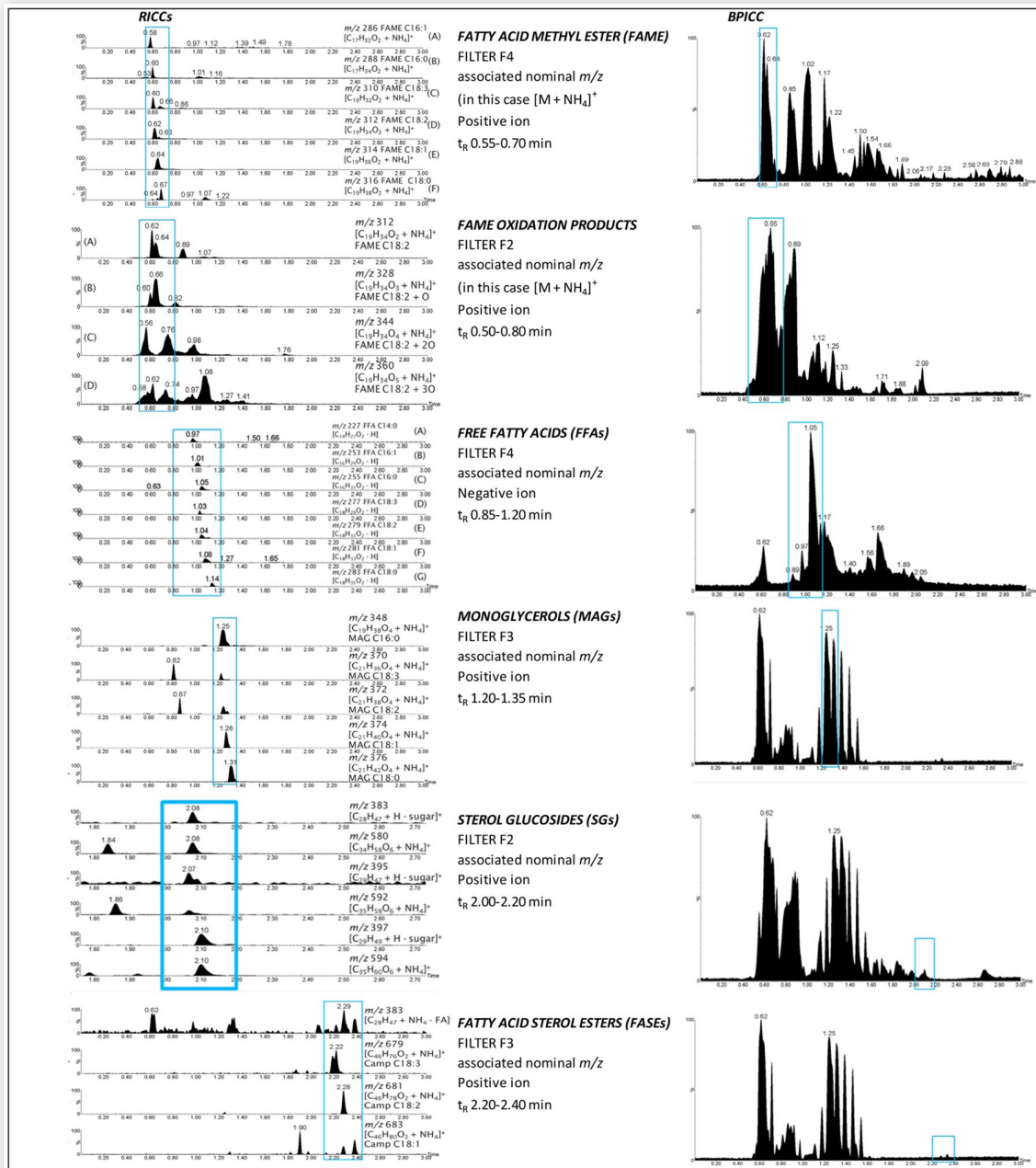


TABLE 1 FAME Molecular formulae and masses

FAMES (Carbon number of double bonds)	Molecular formula, exact mass and structure	Expected m/z (nominal for UHPSFC-MS, monoisotopic for FT-ICR-MS)		
		$[M+H]^+$	$[M+NH_4]^+$	$[M+Na]^+$
C16:1	<chem>C17H32O2</chem> , 268.24 g/mol 	269.2475	286 (t_R : 0.58 min)	291.2301
C16:0	<chem>C17H34O2</chem> , 270.26 g/mol 	271.2636	288 (t_R : 0.60 min)	293.2456
C18:3	<chem>C19H32O2</chem> , 292.24 g/mol 	293.2480	310 (t_R : 0.60 min)	315.2295
C18:2	<chem>C19H34O2</chem> , 294.26 g/mol 	295.2636	312 (t_R : 0.62 min)	317.2451
C18:1	<chem>C19H36O2</chem> , 296.27 g/mol 	297.2791	314 (t_R : 0.64 min)	319.2608
C18:0	<chem>C19H38O2</chem> , 298.29 g/mol 	299.2945	316 (t_R : 0.68 min)	321.2765

$[M + NH_4]^+$ observed at nominal m/z 286-316, consistent with FAMES nominal masses.

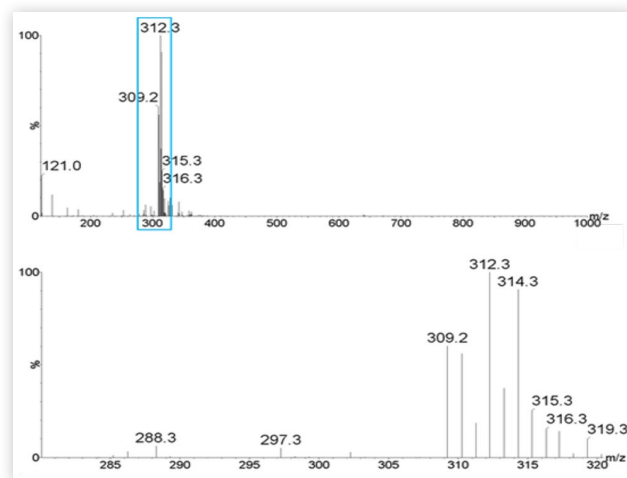
RICCs for FAMES and their associated nominal m/z values (in this case $[M + NH_4]^+$ as shown in Table-2, suggesting that the respective peaks are related to the C16:1, C16:0, C18:3, C18:2, C18:1 and C18:0 FAMES.

Figure 6 shows sodiated molecules observed for FAMES C16:1, C16:0, C18:3, C18:2, C18:1 and C18:0 when using direct infusion positive ion ESI FT-ICR MS Table 1. This agrees with proposed FAMES observed in the positive ion ESI UHPSFC-MS data for F4, with the sodium adducts further confirming presence of FAME species with accurate mass measurements providing confidence in compound assignments.

Nominally isobaric species are observed with both $[C16:0 + Na]^+$ and $[C18:3 + H]^+$ at nominal m/z 293.

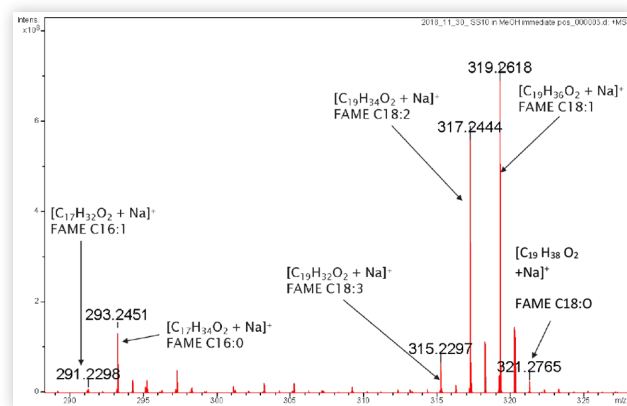
Fatty Acid Methyl Ester (FAME) Oxidation Products The filter sample F2 will be used to illustrate the FAME oxidation products found within the fuel filter samples.

Table 2 shows a summary of the FAMES and their respective molecular formulae, adducts that may be present and their associated masses based on previous studies [17, 18]. Each

FIGURE 5 Positive ion ESI UHPSFC mass spectrum of fuel Filter F4 at t_R 0.55-0.70 min, mass range, m/z 120-1000, zoomed range m/z 280-320

FAME has been given a designated colour dependent on number of double bonds, which are a match for the coloured arrows in figures 5 and 6. The BPICC showed Figure 4, ions consistent with the respective FAME oxidation products up to the addition of three additional oxygen atoms were also observed, in agreement with Table 2.

FAMES and FAME oxidation products were found to elute between t_R 0.50-0.80 min (yellow box), as shown in

FIGURE 6 Direct infusion positive ion ESI FT-ICR-MS spectrum of fuel filter F4 (zoomed m/z 290-330) showing sodiated molecules for FAMES**TABLE 2** FAME Molecular formulae and masses

FAMES (carbon number: number of double bonds)	Molecular formula	Expected m/z (nominal for UHPSFC-MS, monoisotopic for FT-ICR MS)									
		$[M+H]^+$	$[M+NH_4]^+$	$[M+Na]^+$	$[(M+O)+NH_4]^+$	$[(M+O)+Na]^+$	$[(M+2O)+NH_4]^+$	$[(M+2O)+Na]^+$	$[(M+3O)+NH_4]^+$	$[(M+3O)+Na]^+$	
C18:3	<chem>C19H32O2</chem>	293.248	310	315.23	326	331.225	342	347.2197	358	363.2147	
C18:2	<chem>C19H34O2</chem>	295.263	312	317.246	328	333.24	344	349.2354	360	365.2307	
C18:1	<chem>C19H36O2</chem>	297.279	314	319.262	330	335.256	346	351.2506	362	367.246	

Figure 3. The corresponding positive ion ESI UHPSFC mass spectrum shown in **Figure 8** shows ammoniated molecules $[M + NH_4]^+$ in agreement with FAMES and FAME oxidation product nominal masses as shown in **Table 2**.

RICCs for nominal m/z associated with FAME C18:2 and associated FAME oxidation products (in this case $[M + NH_4]^+$ as shown in **Figure 4** is shown in **Figure 7**, to confirm the assignment.

The main differences are fuel filter F2 was only observed to have FAME oxidation products with the addition of one oxygen atom, whereas fuel filter F3 was observed to have FAME oxidation products up to the addition of two oxygen atoms.

The major similarities are FAME containing fuel filters have FAME oxidation products observed at C18:3, C18:2 and C18:1 with varying additions of oxygen. Data for fuel filters F1 and F3 showed the presence of FAMES with up to three additional oxygen atoms.

The presence of FAME oxidation products suggests that the fuels passing through F1, F2, F3 and F4 have oxidized. The difference in abundances of FAME oxidation products observed corresponds to the different extent of oxidation each fuel will have undergone. The trace levels of FAMES in F3

FIGURE 7 Direct infusion positive ion ESI FT-ICR-MS data of fuel filter F2 (zoomed m/z 310-370), showing sodiated products for C18 and C18 oxidation products up to the addition of three oxygen atoms.

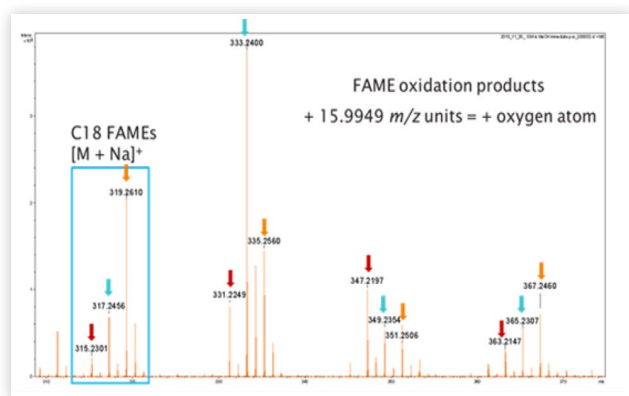
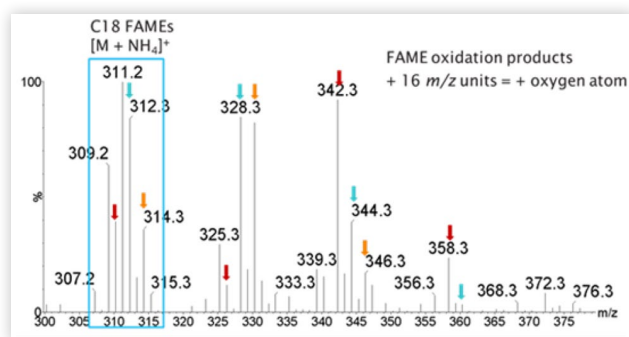


FIGURE 8 Positive ion ESI UHPSFC mass spectrum of F2 at t_R 0.50-0.80 min (zoomed m/z 300-380), showing ammoniated molecules for C18 FAMES and their respective FAME oxidation products.



could suggest that almost all FAMES have oxidized to FAME oxidation products as in F4.

FAME oxidation products have been linked to filter fouling and blocking as well as both aged fuel IDIDs and metal salt IDIDs [19, 20, 21]. Oxidative stress has been found to cause the formation of insoluble and deposits causing filter plugging, injector blockage and component failure [26].

Free Fatty Acids Free fatty acids may be a byproduct of FAME production in biodiesel [20, 23, 24, 25], or present in petrodiesel/biodiesel blends as a lubricity additive or corrosion inhibitor [24]. The F4 fuel filter will be used as the example to illustrate FFAs within fuel filter samples.

Table 3 shows a summary of the FFAs, their respective molecular formulae, exact mass and structure, the adduct that can be present for each and their associated masses [262].

FFAs were found to elute at t_R 0.85 - 1.20 min as shown in **Figure 3**. The corresponding negative ion ESI UHPSFC mass spectrum shown in **Figure 9**, shows deprotonated molecules $[M - H]^-$ observed at nominal m/z values matching those in **Table 3**. RICCs of associated m/z values for FFAs (in this case $[M - H]^-$ as shown in **Figure 4**), are consistent with C14:0, C16:1, C16:0, C18:3, C18:2, C18:1 and C18:0 FFAs.

FFAs were also observed as deprotonated molecules $[M - H]^-$ in fuel filter F4 (m/z values in **Table 3**) using direct infusion negative ion ESI FT-ICR MS as shown in **Figure 10**. The

TABLE 3 Free acids molecular formulae and masses

m/z	m/z	m/z (nominal-for-UHPSFC-MS, monoisotopic-for-FT-ICR-MS)
FFA η (Carbon-number; number-of-double-bonds) η	Molecular-formula, exact-mass-and-structure η	$[M-H]^-$ η
C14:0 η	$C_{14}H_{28}O_2$, 228.21-g/mol η 	227.2022 η (t_R : 0.96-min) η
C16:1 η	$C_{16}H_{30}O_2$, 254.22-g/mol η 	253.2180 η (t_R : 1.02-min) η
C16:0 η	$C_{16}H_{32}O_2$, 256.24-g/mol η 	255.2337 η (t_R : 1.05-min) η
C18:3 η	$C_{18}H_{30}O_2$, 278.22-g/mol η 	277.2182 η (t_R : 1.03-min) η
C18:2 η	$C_{18}H_{32}O_2$, 280.24-g/mol η 	279.2339 η (t_R : 1.04-min) η
C18:1 η	$C_{18}H_{34}O_2$, 282.26-g/mol η 	281.2496 η (t_R : 1.09-min) η
C18:0 η	$C_{18}H_{36}O_2$, 284.27-g/mol η 	283.2652 η (t_R : 1.14-min) η

FIGURE 9 Negative ion ESI UHPSFC mass spectrum of fuel filter F4 at t_R 0.85-1.15 min (zoomed m/z 180-300)

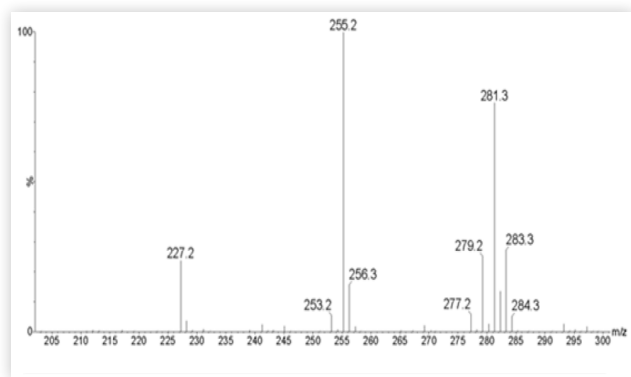
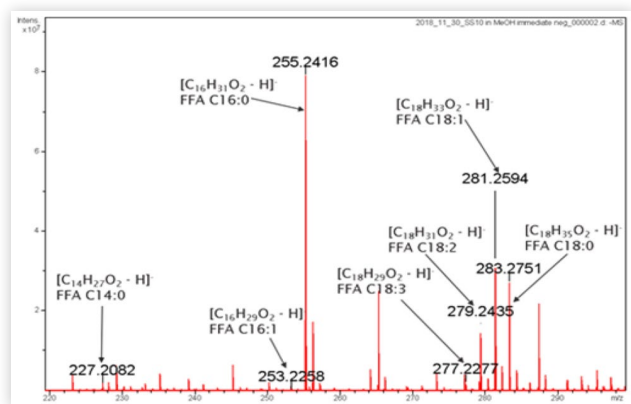


FIGURE 10 Direct infusion negative ion ESI-FT-ICR mass spectrum of F4 (zoomed m/z 180-300) showing deprotonated molecules for FFAs.



accurate mass data provides further confidence that C14:0, C16:1, C16:0, C18:3, C18:2, C18:1 and C18:0 FFAs were observed in F4 in agreement with negative ion ESI UHPSFC-MS.

FFAs are well known as a contributing compound for metal carboxylates deposits both in fuel filter and fuel injector IDIDs [25,27].

Monoglycerols (MAGs) Monoacylglycerols (MAGs) consist of a glycerol linked *via* an ester bond to a fatty acid [28]. MAGs are present as minor constituents or contaminants, within biodiesel as a byproduct of incomplete transesterification [29].

Saturated MAGs have been found to plug fuel filters due to the low solubility of MAGs in biodiesel leading to the formation of solid precipitates in cold weather [1, 30, 31].

Table 4 shows a summary of the MAGs, their respective molecular formulae and structures, adducts that can be present and their associated masses [26] with nominally isobaric species m/z in bold and underlined.

The F3 fuel filter will be used as the example to illustrate MAGs within fuel filter samples.

MAGs were found to elute at t_R 1.20-1.35 min with the corresponding positive ion ESI UHPSFC mass spectrum

TABLE 4 MAGs molecular formulae and masses

n	n	Expected m/z (nominal for SFC, monoisotopic (+dp) for FT) n		
		$[M+H]^+$ n	$[M+NH_4]^+$ n	$[M+Na]^+$ n
MAGs n	(Carbon number, number of double bonds) n	Molecular formula, exact mass and structure n		
C16:0 n	<chem>CCCCCCCCCCCCCCCC(=O)OCC(O)CO</chem>	331.2843 n	348 n (t_R : 1.25 min) n	<u>353.2662</u> n
C18:3 n	<chem>CCCC=CCCC=CCCC=CCCC(=O)OCC(O)CO</chem>	<u>353.2686</u> n	370 n (t_R : 1.23 min) n	375.2506 n
C18:2 n	<chem>CCCC=CCCC=CCCCCCCC(=O)OCC(O)CO</chem>	355.2843 n	372 n (t_R : 1.25 min) n	377.2662 n
C18:1 n	<chem>CCCC=CCCCCCCCCCCC(=O)OCC(O)CO</chem>	357.2999 n	374 n (t_R : 1.28 min) n	379.2819 n
C18:0 n	<chem>CCCCCCCCCCCCCCCCCCCC(=O)OCC(O)CO</chem>	359.3156 n	376 n (t_R : 1.31 min) n	381.2975 n

shown in Figure 11, shows a mixture of protonated $[M+H]^+$ and ammoniated $[M+NH_4]^+$ molecules with nominal masses in agreement with MAGs nominal masses in Table 5.

RICCs of associated m/z values for MAGs ($[M+NH_4]^+$) as shown in Figure 4 suggests that the respective peaks are related to MAGs C16:0, C18:3, C18:2, C18:1 and C18:0

MAGs are observed as sodiated molecules $[M+Na]^+$ using direct infusion positive ion ESI FT-ICR MS, Figures 12, 13 and 14.

Dimeric MAG species are also observed as sodiated molecules $[2M+Na]^+$ and are most likely artefacts formed during the ESI process, rather than present in the fuel filter sample. Dimers often suggests a component is present at a high concentration, therefore sample dilution is required.

To further confirm the assignment of MAGs, MS/MS was undertaken on F3 fuel filter sample.

Tandem MS Alongside accurate mass measurements obtained using positive ion ESI FT-ICR MS, tandem MS (MS/MS) was undertaken on F3 to further fully characterize the

FIGURE 11 Positive ion ESI UHPSFC mass spectrum of fuel filter F3 at t_R 1.20-1.35 min (zoomed range m/z 235-390)

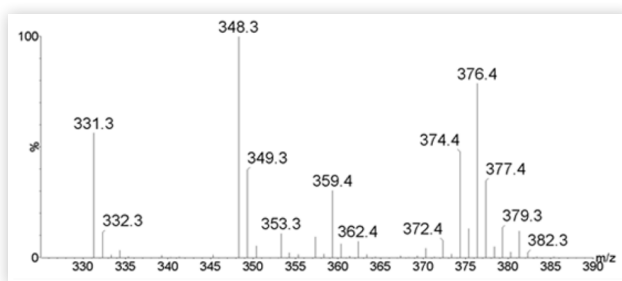


FIGURE 12 Direct infusion positive ion ESI FT-ICR spectrum of fuel filter F3, (zoomed m/z 100-1000), showing sodiated molecules for MAGs and MAG dimers.

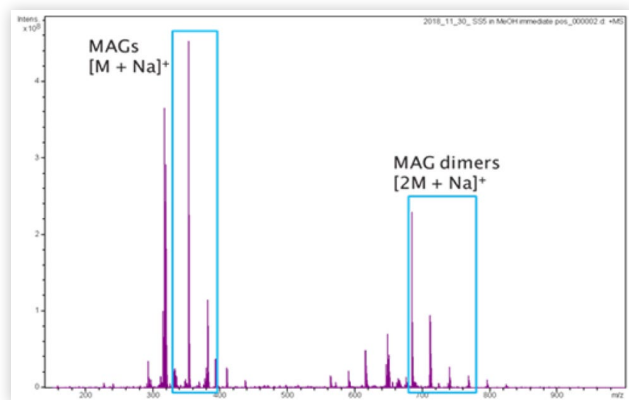


FIGURE 13 Direct infusion positive ion ESI FT-ICR mass spectrum of fuel filter F3 (zoomed m/z 340-390)

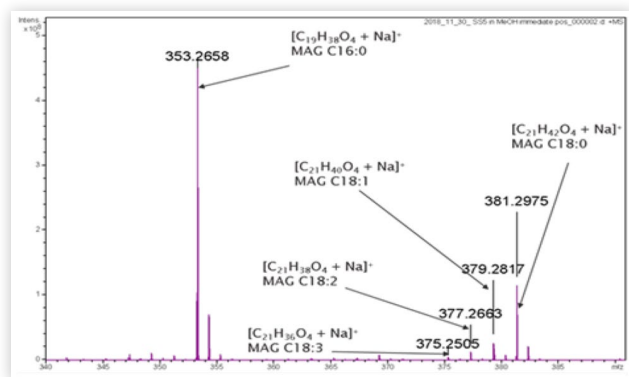
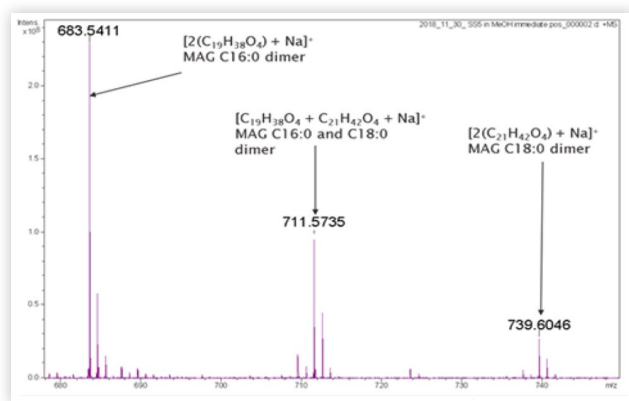


FIGURE 14 Direct infusion positive ion ESI-FT-ICR mass spectrum of fuel filter F3 (zoomed m/z 680-750), showing sodiated molecules for MAGs.



suspected MAG species within the sample. UHPSFC with positive ion electrospray ionization mass spectrometry/mass spectrometry. A triple quadrupole (QQQ) mass spectrometer was used.

The masses for the ammoniated molecules $[M + NH_4]^+$ of interest, in this case, m/z 348, 370, 372, 374, 376 as shown

in [Figure 11](#), were individually isolated and then fragmented in the collision cell. The resulting product ions were then detected [Figures 15](#) and [16](#)

Three different collision energies were considered; 5, 10 and 20 V, with 5 V being considered optimal for fragmentation to produce product ions. Two examples, MAG C16:0, [Figure 12](#), and MAG C18:0, [Figure 14](#), will be discussed in detail.

The product ion scan for m/z 348 [figure 14](#) is consistent with the precursor ion for MAG C16:0 ammoniated molecules at m/z 348 $[C_{19}H_{38}O_4 + NH_4]^+$. It has four product ions related to it; m/z 331, m/z 313, m/z 257 and m/z 239.

The ion at m/z 331 is consistent with $[C_{19}H_{38}O_4 + NH_4 - NH_3]^+$, and the loss of 18 m/z units resulting in m/z 313 is consistent with the loss of H_2O from this fragmentation ion.

Additionally, a neutral loss of 92 m/z units (m/z 239) is consistent with loss of glycerol from m/z 331 via a rearrangement and hydrogen transfer.

m/z 257 is consistent with simple charge site cleavage to give $([MAG + NH_4 - NH_3 - glyceride])^+$.

The product ion scan for m/z 374 [figure 16](#) is consistent with the precursor ion for MAG C18:1 ammoniated molecule $[C_{21}H_{40}O_4 + NH_4]^+$. It has four key product ions related to it; m/z 357, m/z 339, m/z 283 and m/z 265.

The ion at m/z 357 is consistent with $[C_{21}H_{40}O_4 + NH_4 - NH_3]^+$, and the loss of 18 m/z units resulting in m/z 339 is consistent with the loss of H_2O from this fragmentation ion. A neutral loss of 92 m/z units (m/z 265) is consistent with loss of glycerol from m/z 357 via a rearrangement and hydrogen

FIGURE 15 Product ion mass spectrum of fuel filter F3 of precursor nominal m/z 348 MAG C16:0 $[C_{19}H_{38}O_4 + NH_4]^+$ at t_R 1.11min (TQD) (zoomed m/z 120-400) CE 5 V.

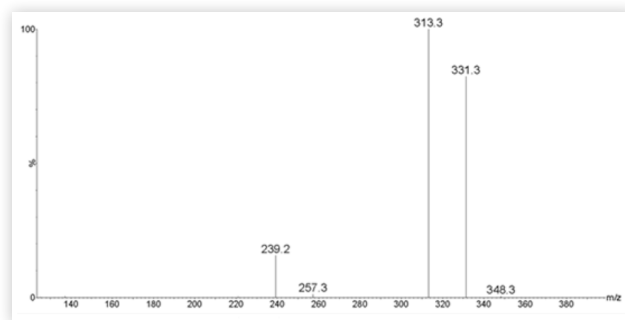
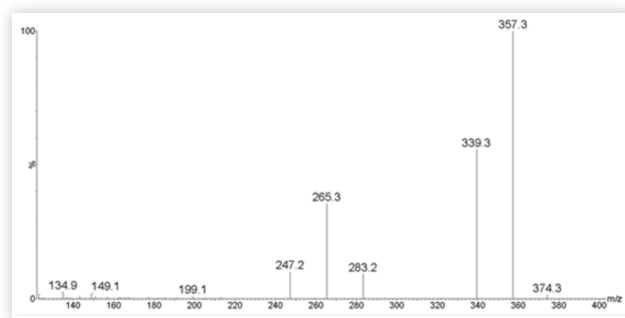


FIGURE 16 Product ion mass spectrum of fuel filter F3 of precursor nominal m/z 374 MAG C18:1 $[C_{21}H_{40}O_4 + NH_4]^+$ at t_R 1.16 min (TQD) (zoomed m/z 120-400) CE 5 V



transfer, m/z 283 is consistent with simple charge site cleavage to give $([MAG + NH_4 - NH_3 - glyceride]^+)$.

The major differences observed were all MAGs were only observed at low level in fuel filter F4, with the complete absence of MAG C18:3.

The key similarities are that fuel filters F1 and F3 both have all MAGs present with dimers. In addition, C16:1, C16:0, C18:3, C18:2, C18:1 are present in fuel filters F1, F3 and F4.

The presence of MAGs in fuel filters suggests the biodiesel blended into the related fuels was a result of an incomplete transesterification reaction. The literature shows the link between MAGs and filter blocking.

In 1996, creamy pastes found to contain MAGs were extracted from plugged filters from buses in Iowa. In the USA, it was reported in winters 2004-2006 that ferry boats fueled by B20 blends were experiencing issues with solid precipitates plugging filters and the solid residues were found to be mainly composed of saturated MAGs [1,2]. Along with SGs, saturated MAGs have been found to form solid precipitates in cold weather due to low solubility of MAGs in biodiesel [2].

MAGs are amphiphilic and may react with any water present in the fuel, with alcohol 'head' of the chain being hydrophilic and more soluble in water while the carbon chain 'tail' is hydrophobic, therefore more soluble in the non-polar petrodiesel. Biodiesel blends result in decreased solubility and accelerated precipitation. Industry tests cloud point (CP), pour point (PP) and cold filter plugging point (CFPP) are used to evaluate cold flow properties of a fuel to predict the tendency for the formation of the solid precipitates from the biodiesel blends. At temperatures even above the CP (temperature at which crystals become visible), precipitates can settle in storage tanks and during and after fuel transfer causing restricted flow and blockages (PP temperature) [32].

Sterol Glucosides Sterol glucosides (SGs) consist of a sterol linked at the hydroxyl group (by a glycosidic bond) to a sugar [29,33]. The F1 fuel filter will be used as the example to illustrate SGs within fuel filter samples.

Table 5 shows a summary of the SGs, their respective molecular formulae and structures, adducts that can be present and their associated masses [34, 35, 36].

Figure 3 shows a positive ion ESI UHPSFC-MS BPICC of the F1 fuel filter, with the red box box highlighting chromatographic peaks within the region of retention found for SGs (t_R 2.00 - 2.20 min).

Figure 17 shows ammoniated molecules $[M + NH_4]^+$ observed at nominal m/z 580-600, which are consistent with compounds of nominal mass 557-577 g/mol. Sterol fragment ions, corresponding to the protonated molecules $[M + H - sugar]^+$ are also observed at nominal m/z 380-400.

Confirmation that the chromatographic peaks in this region are most likely related to SGs and their associated nominal m/z values, in this case $[M + NH_4]^+$ and $[M + H - sugar]^+$ as shown in Table 5 is achieved using RICCs. Table 2, shows RICCs and allows alignments/matchings of sterol fragment ions to the associated SG to be achieved (e.g. for campesteryl glucoside m/z 383 $[M + H - sugar]^+$ and m/z 580 $[M + NH_4]^+$). This suggests that the respective peaks are related to SGs and agrees with previous findings of Patel [37] adding to the confidence in the assignment.

TABLE 5 SGs Molecular formulae and masses

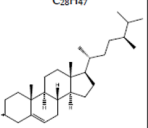
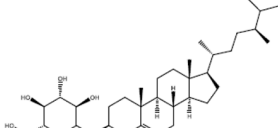
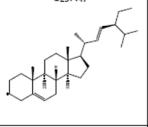
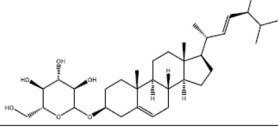
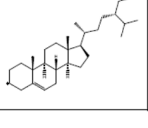
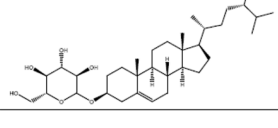
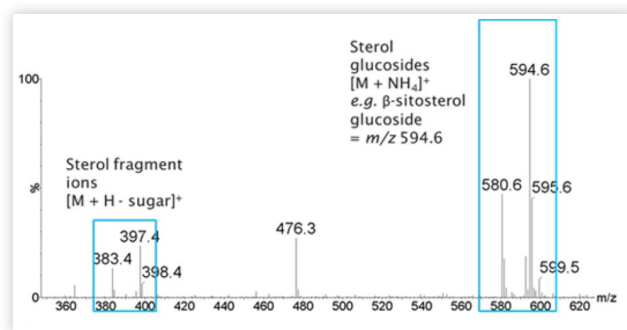
m/z (nominal for UHPSFC-MS, monoisotopic for FT-ICR MS)					
Sterol glucosides	Molecular formula and structure of sterol fragment ion	$[M + H - sugar]^+$ sterol fragment	Molecular formula, exact mass and structure of sterol glucoside	$[M + NH_4]^+$ sterol glucoside	$[M + Na]^+$ sterol glucoside
Campesterol glucoside	<chem>C28H47+</chem> 	383.3672	<chem>C34H58O6</chem> , 562.42 g/mol 	580 (t_R : 2.08 min)	585.4119
Stigmasterol glucoside	<chem>C29H47+</chem> 	395.3672	<chem>C35H58O6</chem> , 574.42 g/mol 	592 (t_R : 2.07 min)	597.4126
β -sitosterol glucoside	<chem>C29H49+</chem> 	397.3829	<chem>C35H50O6</chem> , 576.44 g/mol 	594 (t_R : 2.10 min)	599.4282

FIGURE 17 Positive ion ESI UHPSFC mass spectrum of fuel filter F1 at t_R 2.04-2.14 min zoomed m/z 350-625)



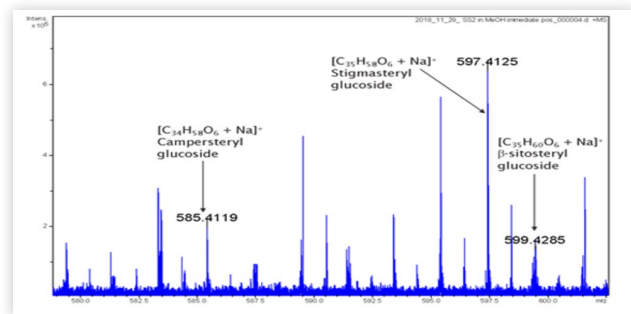
SGs were not easily observed by direct infusion positive ion ESI FT-ICR MS but found to be present at low abundance as the sodiated molecules $[M + Na]^+$, as shown in Figure 18. However, the sterol fragment ions were not observed as protonated molecules $[M + H - sugar]^+$ as previously observed by positive ion ESI UHPSFC-MS, most likely due to the low abundance and possible ion suppression.

SGs were observed to be present in F1 and F2 fuel filters and at very low abundance in F3 fuel filter samples possibly due to presence of fatty acid sterol esters (FASEs).

It was much easier to see SGs by positive ion ESI UHPSFC-MS compared to direct infusion positive ion ESI FT-ICR MS due to absence of ion suppression.

Fatty Acid Sterol Esters (FASEs) Fatty acid sterol esters (FASEs) consist of a sterol linked at the hydroxyl group (via an ester bond) to a fatty acid. FASEs are naturally

FIGURE 18 Direct infusion positive ion ESI FT-ICR mass spectrum of fuel filter F1 (zoomed m/z 580-600) showing sodiated molecules for SGs.



occurring in vegetable oils and biodiesel feedstocks and are therefore found as minor constituents/contaminants within biodiesel, [29, 37.]

This FASEs method was based upon a novel positive ion ESI UHPSFC-MS detection method involving ammonium acetate and demonstrates the novel detection of FASEs in diesel fuel blends. Prior to this FASEs have only been analyzed in pure biodiesel and vegetable oils [38-40.]. FASEs are also not stated in the literature to have been investigated or found to cause filter blocking or IDIDs. However, knowledge that SGs and FFAs are deposit forming compounds suggests FASEs may also be a possible deposit forming precursor or component with work by Feld and Oberender [41] showing FASEs from biodiesel forming deposits after SGs have initially accumulated in fuel filters. Further research is required surrounding their role in biodiesel blends and forming deposits.

The FASEs are only observed by positive ion ESI UHPSFC-MS and they were not apparent by direct infusion positive ion ESI FT-ICR MS again possibly due to ion suppression.

The F3 fuel filter will be used as the example to illustrate detection and identification of FASEs within fuel filter samples.

FASEs are observed most abundantly as ammoniated molecules $[M + NH_4]^+$. Related sterol fragment ions are also observed but as protonated molecules $[M + H - \text{fatty acid}]^+$ using positive ion ESI UHPSFC-MS. Figure 3 shows the chromatographic region for FASEs, (t_R 2.20-2.40 min), highlighted by a dark blue box.

Figure 19, shows ammoniated molecules $[M + NH_4]^+$ observed at nominal m/z 678-696, which are consistent with

FIGURE 19 Positive ion ESI UHPSFC mass spectrum of fuel filter F3 at t_R 2.20-2.40 min.

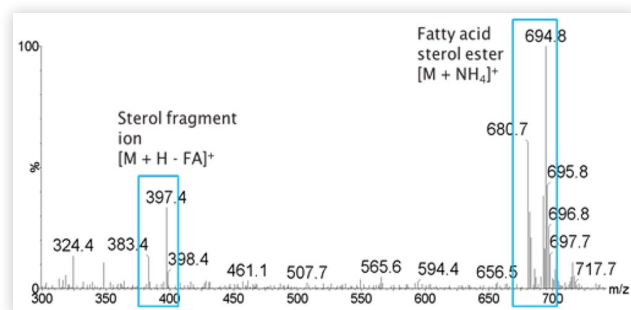


FIGURE 20 Scanning electron micrograph of F1

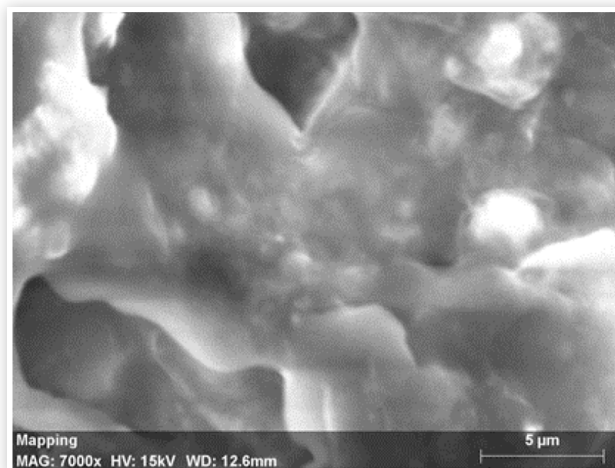


FIGURE 21 Energy Dispersive X-Ray Analysis of filter F1

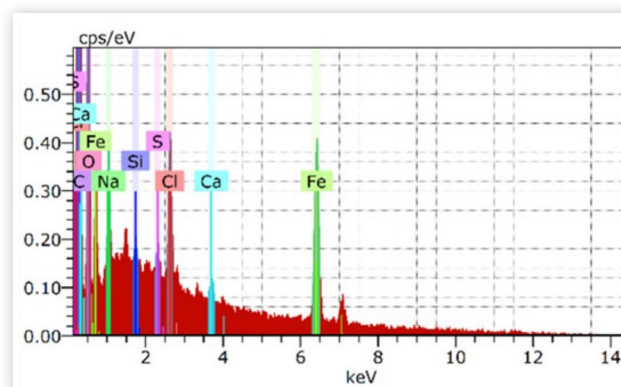


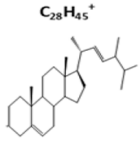
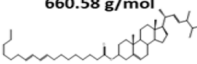
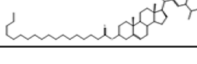
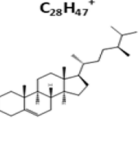
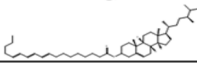
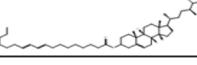
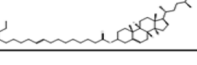
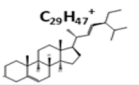
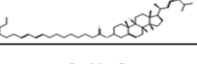
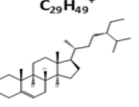
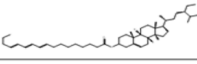
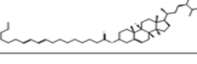
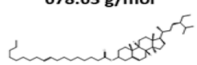
FIGURE 22 Energy Dispersive X-Ray Analysis map of filter F1



compounds of nominal mass 660-678 g/mol. Fragment ions $[M + H - \text{fatty acid}]^+$ are also observed at nominal m/z 381-397, which are consistent with compounds of nominal mass 380-396 g/mol. Both of which are in agreement with FASEs nominal masses as shown in Table 6.

Campesterol ester C18:3, C18:2 and C18:1 and β -sitosterol ester C18:3, C18:2 and C18:1 only were observed to be present

TABLE 6 FASEs Molecular formulae and masses

Fatty acid sterol esters	Sub compounds (degree of saturation)	Molecular formula and structure of sterol fragment ion	[M + H – fatty acid] ⁺ sterol fragment ion	Molecular formula, exact mass and structure of sterol ester	[M + NH ₄] ⁺ sterol ester
Brassicasterol ester	18:02	 C ₂₈ H ₄₅ ⁺	381	C ₄₆ H ₇₆ O ₂ 660.58 g/mol 	678 (t _R :2.09 min)
	18:00		381	C ₄₆ H ₈₀ O ₂ 664.62 g/mol 	682 (t _R :2.16 min)
Campesterol ester	18:03	 C ₂₈ H ₄₇ ⁺	383	C ₄₆ H ₇₆ O ₂ 660.58 g/mol 	678 (t _R :2.09 min)
	18:02		383	C ₄₆ H ₇₈ O ₂ 662.60 g/mol 	680 (t _R :2.17 min)
	18:01		383	C ₄₆ H ₈₀ O ₂ 664.62 g/mol 	682 (t _R :2.24 min)
stigmasterol ester	18:02	 C ₂₉ H ₄₇ ⁺	395	C ₄₇ H ₇₈ O ₂ 674.60 g/mol 	692 (t _R :2.14 min)
β-sitosterol ester	18:03	 C ₂₉ H ₄₉ ⁺	397	C ₄₇ H ₇₈ O ₂ 674.60 g/mol 	692 (t _R :2.14 min)
	18:02		397	C ₄₇ H ₈₀ O ₂ 676.62 g/mol 	692 (t _R :2.20 min)
	18:01		397	C ₄₇ H ₈₂ O ₂ 678.63 g/mol 	696 (t _R :2.29 min)

in the fuel filter F3 No fatty acid brassicasterol ester or stigmasterol esters were found to be present.

It may be possible that a poor source of biodiesel was used in fuel passing through F3 causing the plugged fuel filter and associated residue, or it may be more related to an accumulation issue which may explain why it was only observed in one fuel filter deposit.

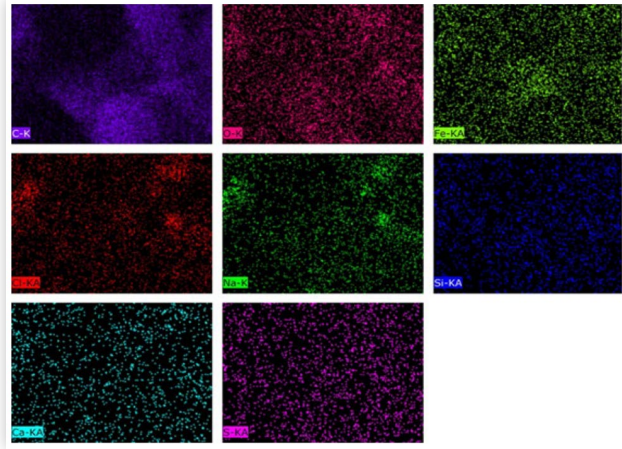
This is the first time FASEs have been identified in petrodiesel/biodiesel blends and strongly suggests that research is required surrounding their role in biodiesel blends and forming deposits.

SEM EDAX

Since this is not the primary focus for this paper, we will simply show its ability in the case of FAME impurities to show counterions or not to the free carboxylic acids found in FAME.

The SEM-EDAX data shows the morphology; granularity and the distribution; across the filter media; and elements which may be involved with the FAME based deposits. Sodium and calcium. The sodium showing some clustering relative to calcium.

FIGURE 23 Energy Dispersive X-Ray Analysis Elemental Maps



FTIRM

The FTIRM data shows that species are varying across the filter medium and different species are present. This is shown by the presence of OH vibration at 3300 cm^{-1} , ester/acid groups around 1732 cm^{-1} , carboxylates at 1603 cm^{-1} . The work of Fang and McCormick [42] has shown that biodiesel can degrade through a number of reaction pathways, methyl ester decomposition, ester hydrolysis and reverse transesterification’s infra-red data described shown indicates some of these mechanisms have occurred in the “field”.

Summary

The data shows the wide spread of impurities across each filter found. Including FAME constituents with differing double bond contents and a complex bioorganic molecules.

FIGURE 24 Photograph of F1 area of infra-red analysis

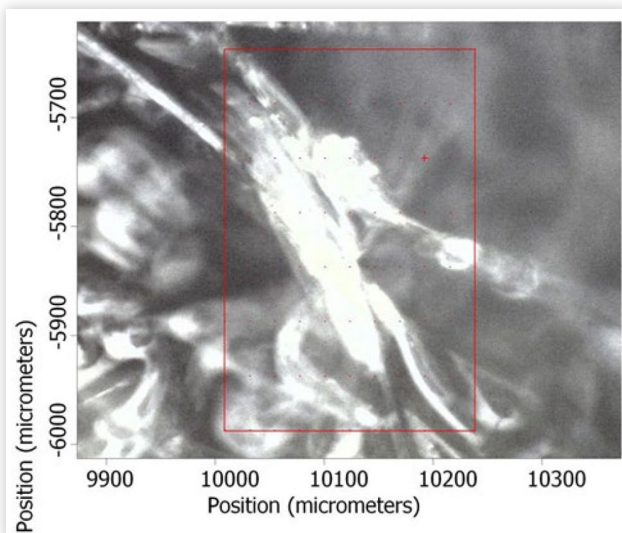


FIGURE 25 Percentage transmittance map (1732 cm^{-1})

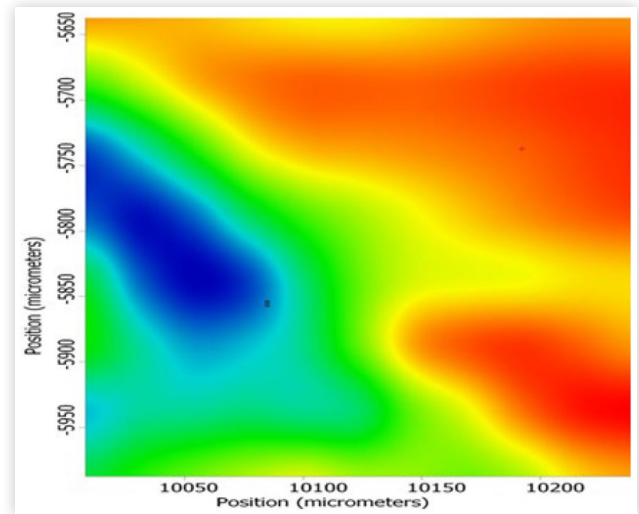
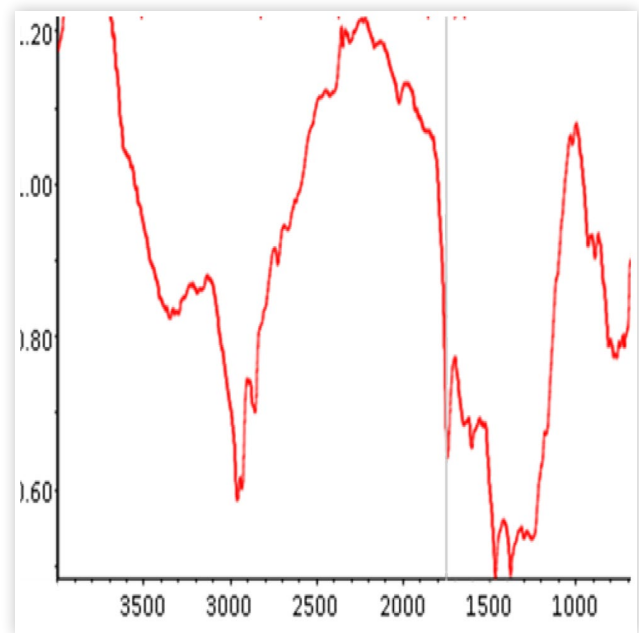


FIGURE 26 Infra-red spectrum of filter deposit.



Conclusions

A rapid methodology has been developed to allow the screening of biocomponents implicated in “field” filter blocking involving FAME species, originating from FAME in petrodiesel/FAME fuel blends. This was without expensive/difficult to source standard materials, using minimal sample and without any sample derivatization steps. These will extend in the future to include different mass spectrometry techniques and other filter blocking species and quantitation.

FASEs have been identified in filter blocking residues from petro diesel biodiesel blends for the first time. Further, because sterol glucosides and free fatty acids are deposit

TABLE 7 Summary of Impurities Found on the Filters

SAMPLE ORIGIN	USE	FAMES	FAME OXIDATION PRODUCTS
1 Northern Europe	Lightduty	(C16:1 and C16:0, C18:3, C18:2, C18:1. traces 18:0)	(C18:3, C18:2, C18:1 only (+1 O,+2 O,+3O))(C14:0, C16:0, C18:3, C18:2, C18:1.and 18:0).
2 UK	light Duty	(C16:1 and C16:0, C18:3, C18:2, C18:1. traces)	(C18:3, C18:2, C18:1 only (+1 O,+2 O,+3O))(C14:0, C16:0, C18:3, C18:2, C18:1.and 18:0).
3 Northern Europe	Light duty	(C16:1 and C16:0, C18:3, C18:2, C18:1, traces 18:0.)	(C18:3, C18:2, C18:1 only (+1 O and +2 O))(C16:0, C18:2, C18:1.and 18:0).
4 Southern Europe	Medium Duty	(C16:1 and C16:0, C18:3, C18:2, C18:1, 18:0).	(C18:3, C18:2, C18:1 only (+1 O)(+2O & +3O low abundance))(C16:1, C16:0, C18:2, C18:1.and 18:0)
SAMPLE ORIGIN	USE	Free Fatty Acids	SGs
1 Northern Europe	Lightduty	C14:0,C16:0,C18:3,C18:2,C18:1 and C18:0	(Campesterol glucoside, β -sitosterol glucoside and low abundance of Stigmasterol glucoside)
2 UK	light Duty	C14:0,C16:0,C18:3,C18:2,C18:1, and C18:0.	(Campesterol glucoside, β -sitosterol glucoside and very low abundance of Stigmasterol glucoside)
3 Northern Europe	Light duty	C16:0,C18:3,C18:2,C18:1, and C18:0	(All very low abundance of campesterol glucoside, β -sitosterol glucoside and Stigmasterol glucoside)
4 Southern Europe	Medium Duty	C16:1,C16:0,C18:3,C18:2,C18:1, and C18:0	
SAMPLE ORIGIN	USE	MGs	FASEs
1 Northern Europe	Lightduty	(C16:0, C18:3, C18:2, C18:1, C18:0. Dimers at m/z 683, 711, 739)	
2 UK	light Duty	(C16:0, C18:3, C18:2, C18:1, C18:0. Dimers at m/z 683, 711, 739)	
3 Northern Europe	Light duty		(Campesterol ester C18:3, C18:2 and C18:1and β - sitosterol ester C18:3, C18:2 and C18:1)
4 Southern Europe	Medium Duty	(C16:0, C18:2, C18:1, C18:0.(low abundance))	

forming compounds and that acylated sterol glucosides become less soluble in biodiesel upon loss the fatty acid chain during esterification FASEs may be molecules of concern regarding filter blocking.

Such methodology has applications as a “suitability for use” of biodiesel and petro diesel/biodiesel blends and will be the subject of further publications.

In recent years the species attributable to biodiesel involved in filter blocking has grown [49], this work adds to that list and may help to aid the understanding of filter blocking. Further as the sources of petroleum diesel and biodiesel continue to diversify mass spectrometry is well placed to identify the deposit forming impurities both qualitatively and quantitatively.

In addition, SEM/EDAX and FTIRM have provided support analysis and information on morphology, elements, and functional group distribution in other studies.

References

- Kortba, R., “Bound by Determination,” *Biodiesel Magazine*, 2006, pp. 42-50, accessed March 2022.
- Lee, I., Pfaltzgraf, L.M., Poppe, G.B., Powers E. et al., “The Role of Steroyl Glucosides on Filter Plugging,” *Biodiesel Mag*, 2007, accessed March 2022, <http://www.biodieslmagazine.com/articles/1566/the-role-of-sterol-glucosides-on-filter-plugging>.
- Csontos, B., Berneyer, H., Ererlandsson, A.C., Forsburg, O. et al., “Characterization of Deposits Collected from Plugged Filters,” *SAE Int. J. Adv. & Curr. Prac. in Mobility* 2, no. 2 (2020): 672-680, doi:<https://doi.org/10.4271/2019-24-0140>.
- Fersner, A.S. and Galante-fox, J.M., “Biodiesel Feedstock and Contaminant Contributions to Diesel Fuel Filter Blocking,” *SAE Int J Fuel and Lubr.* 7 (2014): 783-791.
- American Society for Testing and Materials, “Standard Test Method for Determining Filter Blocking Tendency,” ASTM D2068-20, West Conshohocken, PA, USA.
- Jolly, L., Kitano, K., Sakata, I., Strojekw, W. et al., “A Study of Mixed FAME and Trace Component Effects on the Filter Blocking Propensity of FAME and FAME,” *SAE Technical Paper 2010-01-2116*, 2010, <https://doi.org/10.4271/2010-01-2116>.
- Goplan, K., Chuck, C.J., Roy-Smith, C., and Bannister, C.D., “Assessing the Impact of FAME and Diesel Fuel Composition on Stability and Vehicle Filter Blocking,” *SAE Int. J. Adv in Curr. Prac. Mobility* 1, no. 1 (2019): 284-290, doi:[10:4271/2019-01-0049](https://doi.org/10.4271/2019-01-0049).
- Barker, J., Richards, P., Snape, C., and Meredith, W., “Diesel Injector Deposits an Issue That Has Evolved with Engine Technology,” *SAE Technical Paper 2011-01-1923*, 2011, <https://doi.org/10.4721/2011-01-1923>.
- Richards, P., Barker, J., and Cook, S., “Addressing the Issue of Fuel Filter Fouling with recent Changes in Fuel Quality,” *J. ASTM Int.* 6 (2009): 10-14.
- Heiden, R.W., Schrober, S., and Mittlebach, M., “Solubility Limitations of Residual Steryl Glucosides, Saturated Monoglycerides and Glycerol in Commercial Biodiesel Fuels as Determinants of Filter blockages,” *J. Am. Oil Chem. Soc.* 98 (2021): 1143-1165.
- European Committee for Standardization, “Liquid Petroleum Products -Fatty Acid Methyl Esters(FAME) for Use in Diesel Engines and Heating Applications Requirements and Test Methods- EN14214:2012+A2:2019,” 2019.
- American Society for Testing and Materials, “Standard Specification for Biodiesel Fuel Blend Stock (B100) for Middle Distillate Fuels,” West Conshohocken, PA, USA.
- Spanu, M., Barker, J., Reid, J., Scurr, D. et al., “Detailed Characterization of Diesel fuel Filter Deposits by ToF SIMS and other Analytical methods,” in *12th International Colloquium Fuels Conventional and Future Energy for Automobiles*, 2019. Technische Akademie Esslingen Stuttgart/Ostfildern.
- Bernemyr, H., Csontos, B., Hittig, H., and Forsberg, O., “Study of Nozzle Fouling: Deposit Build-up and Removal,” *SAE Technical Paper 2019-01-2231*, 2019, <https://doi.org/10.4271/2019-01-2231>.
- Barker, J., Reid, J., Smith, S.A., Snape, C. et al., “The Application of New Approaches to the Analysis of Deposits from the Jet Fuel Thermal Oxidation Tester (JFTOT),” *SAE Int. J Fuels and Lubr.* 10, no. 3 (2017): 741-755.
- Barker, J., Langley, G., and Richards, P., “Insights into Deposit Formation in High Pressure Diesel Fuel Injection Equipment,” *SAE Technical Paper 2010-01-2243*, 2010, <https://doi.org/10.4271/2010-01-2243>.
- Wicking, C.C., “The Development and Application of Chromatography and Mass Spectrometry Techniques for the Analysis of Biodiesel and Fuel Related Compounds,” *The University of Southampton*, 2013.

18. Alberici, R.M., de Souza, V., Rocha, J.M., De Sa, G.F. et al., "Used Frying Oil: A proper Feedstock for Biodiesel Production?" *BioEnergy Research* 5, no. 4 (2012): 1002-1008.
19. Barker, J., Langley, G., and Richards, P., "Insights into Deposit Formation in High Pressure Diesel Fuel Injection Equipment," SAE Technical Paper [2010-01-2243](https://doi.org/10.4271/2010-01-2243), 2010, <https://doi.org/10.4271/2010-01-2243>.
20. Lacey, P., Gail, S., Kientz, J., Benoist, G. et al., "Fuel Quality and Diesel Injector Deposits," *SAE Int. J. Fuels and Lubr.* 5, no. 3 (2012): 182-195.
21. Urzędowska, W. and Stępień, Z., "Prediction of Threats Caused by High FAME Diesel Fuel Blend Stability for Engine Injector Operation," *Fuel Process. Technol.* 142 (2016): 403-410.
22. Basha, S.A., Gopal, K.R., and Jebaraj, S., "A Review on Biodiesel Production, Combustion, Emissions and Performance," *Renewable and Sustainable Energy Reviews* 13, no. 6-7 (2009): 1628-1634.
23. Richards, P., *Automotive Fuels Reference Book*, 3rd ed. (Warrendale, PA: SAE international, 2014)
24. "ATC Fuel Additives: Use and Benefit," 2013.
25. Lacey, P., Gail, S., Kientz, J., Benoist, G. et al., "Fuel Quality and Diesel Injector Deposits," *SAE Int. J. Fuels and Lubr.* 5, no. 3 (2012): 182-195.
26. Kalo, P.J., Ollilainen, V., Rocha, J.M., and Malcata, F.X., "Identification of Molecular Species of Simple Lipids by Normal Phase Liquid Chromatography-Positive Electrospray Tandem Mass Spectrometry, and Application of Developed Methods in Comprehensive Analysis of Low Erucic Acid Rapeseed Oil Lipids," *Int. J. Mass Spectrom.* 254, no. 1 (2006): 106-121.
27. Trobaugh, C., Burbrink, C., Zha, Y., Whitacre, S. et al., "Internal Diesel Injector Deposits: Theory and Investigations into Organic and Inorganic Based Deposits," *SAE Int. J. Fuels and Lubr.* 6 (2013): 772-784.
28. IUPAC, "Compendium of Chemical Terminology," in: McNaught, A.D., Wilkinson, A. and Chalk, S.J. (Eds), *Gold Book*, 2nd ed., (Oxford: Blackwell Scientific Publications, 1997).
29. Dunn, R.O., "Effects of Minor Constituents on Cold Flow properties and Performance of Biodiesel," *Prog. Energy Combust. Sci.* 35, no. 6 (2009): 481-489.
30. Dunn, R.O., "Effects of Monoacylglycerols on the Cold Flow Properties of Biodiesel," *J. of the Am. Oil Chem. Soc.* 89, no. 8 (2012): 1509.
31. Knothe, G., Krahl, J., and Van Gerpen, J. (Eds), "Fuel Properties," in: , *The Biodiesel Handbook*, 2nd ed., (AOCS Press, 2010), 137-251.
32. Dunn, R.O. and Moser, B.R., "Cold Weather Properties and Performance of Biodiesel," in: Knothe, G., Krahl, J. and van Gerpen, J. (Eds), *The Biodiesel Handbook*, 2nd ed., (AOCS Press, 2010), 147-205.
33. Hoed V., Zyaykina, N., Greyt, W., Maes, J., Vehre,J., Demeestere, K., "Identification and Occurrence of Steroyl Glucosides in Palm and Soy Diesel". *J. Am. Oil Chem. Soc.* 2008, 85,
34. Oppliger, S., Munger, L., and Nystroem, L., "Rapid and Highly Accurate Detection of Steryl Glucosides by Ultraperformance Liquid Chromatography/Quadrupole Time of Flight Mass Spectrometry," *J. Agric. Food. Chem.* 62, no. 4 (2014).
35. Wewer, V., Dombrink, I., vom Dorp, K., and Dörmann, P., "Quantification of Sterol Lipids in Plants by Quadrupole Time-of-flight Mass Spectrometry," *J. Lipid Res.* 52, no. 5 (2011): 1039-1054.
36. Patel, K., "Analysis of Internal Diesel Injector Formation by Separation Science and Mass Spectrometry," Doctoral thesis, University of Southampton, 2016.
37. Hailat, I. and Helleur, E.T.R., "Identification of Fatty Acid Steryl Esters in Margarine and Corn Using Direct Flow Injection ESI MS Ion-Trap Mass Spectrometry," *Int. J. Mass Spectrom.* 362 (2014): 24-31.
38. Plank, C. and Lorbeer, E., "On-line liquid Chromatography Gas Chromatography for the Analysis of Free and Esterified Sterols in Vegetable Oil Methyl Esters used as Diesel Fuel Substitutes," *J. Chromatogr. A* 683, no. 1 (1994): 95-104.
39. Plank, C. and Lorbeer, E., "Minor Components in Vegetable Oil Methyl Esters I: Sterols in Rape Seed Oil Methyl," *Lipid/ Fett* 96, no. 10 (1994): 379-386.
40. Verylen, T., Forcades, M., Verhe, R., Dewettinck, K. et al., "Analysis of Free and Esterified Sterols in Vegetable Oils," *J. of Am. Oil Chem. Soc.* 79, no. 2 (2002): 177-122.
41. Feld, H. and Oberender, N., "Characterization of Damaging Biodiesel Deposits and Biodiesel Samples by Infrared Spectroscopy (ATR-FTIR) and Mass Spectrometry (TOF-SIMS)," *SAE Int. J. of Fuels and Lubr.* 9 (2016): 717-724, doi:<https://doi.org/10.4271/2016-01-9078>.
42. Fang, H.L. and McCormick, R.L., "Spectroscopic Study of Biodiesel Pathways," SAE Technical Paper [2006-01-3300](https://doi.org/10.4271/2006-01-3300), 2006, <https://doi.org/10.4271/2006-01-3300>.

Contact Information

Dr. Jim Barker

Tel: +44 151 355 3611

jim.barker@innospecinc.com

Innospec Limited

Innospec Manufacturing Park, Oil Sites Road, Ellesmere Port.

Cheshire, CH65 4EY, England

<http://www.innospecinc.com>

Acknowledgments

The authors would like to thank Mr. D Knight Innospec for the disassembling the filters and EPSRC for funding Anastarsia Christine Marie-Louise Carter at the University of Southampton.